*J. Braz. Chem. Soc.*, Vol. 19, No. 8, 1501-1512, 2008.
Printed in Brazil - ©2008 Sociedade Brasileira de Química
0103 - 5053 $6.00+0.00

Article

# Synthesis of Fe/Ti Oxides from a Single Source Alkoxide Precursor under Inert Atmosphere

***Pedro H. C. Camargo,[a] Giovana G. Nunes,[a] Eduardo L. de Sá,[a] Germano Tremiliosi-Filho,[b] David J. Evans,[c] Aldo J. G. Zarbin[a] and Jaísa F. Soares*[,a]***

[a]*Departamento de Química, Universidade Federal do Paraná, Centro Politécnico, Jardim das Américas, 81530-900 Curitiba-PR, Brazil*

[b]*Instituto de Química de São Carlos, Universidade de São Paulo, 13560-970 São Carlos-SP, Brazil*

[c]*John Innes Centre, Norwich Research Park, Colney, Norwich NR4 7UH, England*

O alcóxido heterometálico [FeCl{$Ti_2(OPr^i)_9$}] (**1**) foi utilizado como um precursor de fonte única para a preparação de óxidos de Fe/Ti sob atmosfera inerte. Três procedimentos sintéticos distintos foram adotados no processamento de **1**, com o emprego de soluções aquosas ácidas ($HNO_3$ ou HCl), ou na ausência de ácido mineral. Os produtos foram caracterizados por difratometria de raios X (pó), microscopia eletrônica de varredura combinada com espectroscopia de dispersão de raios X (MEV/EDS) e espectroscopias Raman, de ressonância paramagnética eletrônica (RPE) e Mössbauer. Os óxidos produzidos contêm titânio(IV) e ferro(III) (ou ferro(II)), dependendo das condições de reação e das temperaturas de tratamento térmico. Uma interessante redução de ferro(III) a ferro(II), que levou à obtenção de ilmenita ($FeTiO_3$), foi observada a 1000 °C no sistema contendo $HNO_3$. Estudos por MEV/EDS revelaram uma distribuição altamente heterogênea dos metais em todos os produtos, possivelmente relacionada com a presença de um conteúdo significativo de carbono e de defeitos estruturais (vacâncias de oxigênio) nos sólidos.

The heterometal alkoxide [FeCl{$Ti_2(OPr^i)_9$}] (**1**) was employed as a single source precursor for the preparation of Fe/Ti oxides under inert atmosphere. Three different synthetic procedures were adopted in the processing of **1**, either employing aqueous $HNO_3$ or HCl solutions, or in the absence of mineral acids. Products were characterised by powder X-ray diffractometry, scanning electron microscopy combined with energy dispersive X-ray spectroscopy (SEM/EDS) and Raman, electron paramagnetic resonance (EPR) and Mössbauer spectroscopies. Oxide products contained titanium(IV) and either iron(III) or iron(II), depending on reaction conditions and thermal treatment temperatures. An interesting iron(III)→iron(II) reduction was observed at 1000 °C in the $HNO_3$-containing system, leading to the detection of ilmenite ($FeTiO_3$). SEM/EDS studies revealed a highly heterogeneous metal distribution in all products, possibly related to the presence of a significant content of carbon and of structural defects (oxygen vacancies) in the solids.

**Keywords:** oxides, sol-gel, single source precursor, inert atmosphere, electron microscopy

## Introduction

Multimetal oxide systems play an important role in materials science. They have been extensively investigated for the development of high performance ceramics and (nano)composites, aiming at applications in optics, electronics, magnetism and catalysis. The development of structural components, energy conversion devices, sensors and MRI contrast agents has also benefited from heterometal oxide research.[1-4]

Nowadays, the preparation of these oxides is often performed by chemical methods.[3,5-7] In particular, the sol-gel process, either hydrolytic or non-hydrolytic, has been widely employed due to its advantages over conventional solid state methods. These advantages include lower processing temperatures and better control over microstructure, uniformity and stoichiometry of the final material.[3,8,9]

The sol-gel synthesis of heterometal oxides is usually carried out from a mixture of homometal compounds, in which each precursor provides one of the desired metal elements to the final material. The molar ratio of these

*e-mail: jaisa@quimica.ufpr.br

precursors is generally based on the metal proportion in the oxide system of interest.[10,11] More recently, the use of single source precursors (SSPs) has emerged as an alternative for the production of multimetal oxides. SSPs are complexes which contain all necessary metal elements, that is, those required to give the final oxide material, incorporated in the same molecular moiety.[12-15] Depending on a number of factors, such as ligand composition, choice of solvents, stability in processing and metal stoichiometry with respect to the desired product, the use of SSPs can allow the synthesis of pure and homogeneous mixed metal oxides.[5-7]

In earlier reports[16,17] we presented our first results on the sol-gel synthesis of iron-titanium oxides using the structurally characterised $Fe^{II}/Ti^{IV}$ SSP, [FeCl{$Ti_2(OPr^i)_9$}] (**1**, Figure 1).[18] This precursor contains two titanium(IV) centres, each coordinated to six isopropoxide groups, and one iron(II) centre coordinated to four isopropoxides and one chloride. A rutile-$TiO_2$/pseudobrookite ($Fe_2TiO_5$) composite with no phase segregation at a sub-micrometer level was obtained when the sol-gel synthesis from **1** and the thermal treatment were carried out in air.[16] These results were then compared to those given by a 1:2 mixture of $FeCl_2$ and [$Ti(OPr^i)_4$] processed in an analogous way; solids obtained from the mixture of homometal precursors presented significant phase segregation.[17] This indicated that **1** could generate oxide-oxide composites with a degree of homogeneity not achieved by the conventional multicomponent route. More recently, we also reported the use of **1** as the first SSP to give nanocomposites of iron and titanium oxides incorporated in Porous Vycor Glass (PVG).[19]

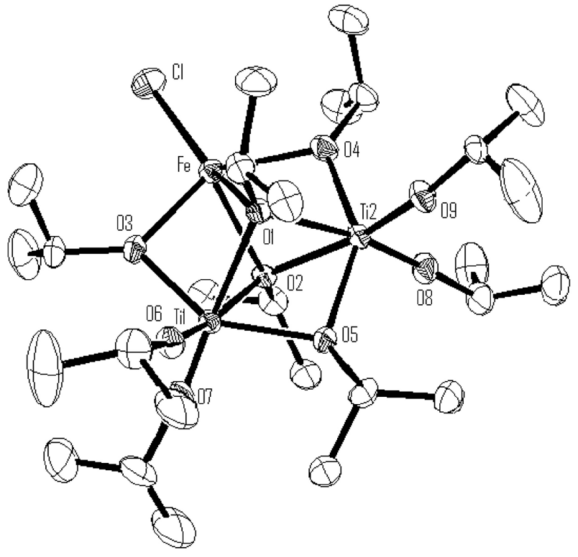


**Figure 1.** ORTEP-3 representation of [FeCl{$Ti_2(OPr^i)_9$}] (**1**).

In this work, we investigate how changes in experimental conditions influence the nature of the sol-gel products obtained from **1**. Here, we specifically analyze the effect, on the final material, of changing hydrolysis conditions (presence of a mineral acid) and of using inert atmosphere during both the hydrolysis/condensation and thermal treatment steps. To the best of our knowledge, this is the first survey on the combined influence of these parameters over the chemical nature and distribution of sol-gel products. Additionally, as **1** contains iron in a relatively low oxidation state ($Fe^{II}$), the use of an inert atmosphere was proposed to minimize oxidation processes in the reaction media, and even change the nature of the composites obtained from the SSP, when compared to the previous preparations carried out in air.[16,19] Results reveal a number of interesting findings which will be described below.

## Experimental

### *General*

Reactions were carried out under $N_2$ (99.999%, Praxair) using standard Schlenk techniques. Commercial reagents and solvents were supplied by Aldrich or Mallinckrodt-Baker. Toluene was dried by standard procedures and distilled prior to use.[20] Anhydrous propan-2-ol (99.5%; septa-sealed bottles under $N_2$) was used as received from Aldrich. [FeCl{$Ti_2(OPr^i)_9$}] was prepared according to our previous report.[18] Aqueous solutions were degassed by bubbling $N_{2(g)}$ for 2 h prior to use. Solids obtained after the sol-gel processing of **1** were submitted to thermal treatment for 2h in a tubular oven (heating rate 30 °C $min^{-1}$) under dinitrogen or argon.

Raman spectra were obtained on a Renishaw Raman Image spectrophotometer coupled to an optical microscope that focuses the incident radiation down to a 1 μm spot. An $Ar^+$ laser (514 nm) with an incident potency of 2 mW was used over the 185-2000 $cm^{-1}$ region.

Electron paramagnetic resonance (EPR) data (X-band, 9.5 GHz) were registered for all solid samples on a Bruker ESP-300E instrument. Measurements were carried out both at room temperature and at 77 K.

Solid state $^{57}$Fe Mössbauer data were recorded in zero field at 80 K on an ES-Technology MS105 spectrometer with an 875MBq $^{57}$Co source in a rhodium matrix. Spectra were referenced against iron foil at 298 K and fitted with Lorentzian curves.

Powder X-ray diffraction (XRD) patterns were obtained on a Shimadzu XRD 6000 diffractometer, using Cu-$K_\alpha$ radiation ($\lambda$ = 1.5418 Å) in the 2$\theta$ range of 10-80°.

Instrument conditions were 40 kV, 40 mA and a scan rate of 2° $min^{-1}$ in 2θ. Measurements were performed at room temperature on samples spread on a conventional glass holder. Powder silicon reflections were used for 2θ calibrations. Crystallite diameters were determined by the use of Scherrer's equation, following Gaussian deconvolution of the XRD peaks.

Scanning electron microscopy and energy dispersive X-ray spectroscopy analyses (SEM/EDS) were performed with a LEO 440 electronic microscope equipped with an Oxford 7060 analyser, assembled with a Pentafet ATW detector (Si-Li crystal) and a polymer-based ultra thin window. The resolution at 5.9 keV is 133 eV and allows the detection of elements down to boron (Z = 5).

*Syntheses from SSP [FeCl{$Ti_2(OPr^i)_9$}], (**1**)*

Codes adopted to designate samples in this paper indicate the atmosphere condition (IN-inert), the thermal treatment temperature and the acid employed. The NC (no catalyst) label was also used when appropriate.

*Hydrolysis and thermal treatment under inert atmosphere, in the presence of $HNO_3$ ($IN/HNO_3$ samples)*

A solution of [FeCl{$Ti_2(OPr^i)_9$}] (1.07 g, 1.49 mmol) in toluene:propan-2-ol (32:64 mL) was added to 32 mL of an aqueous $HNO_3$ solution (0.10 mol $L^{-1}$). This reaction mixture was stirred at 55 °C for 50 h, producing a white suspension which was dried at 55 °C under vacuum to give a brown solid ($IN55/HNO_3$). Portions of $IN55/HNO_3$ were heated at 300, 500, 700 and 1000 °C, giving the solid samples $IN300/HNO_3$, $IN500/HNO_3$, $IN700/HNO_3$ and $IN1000/HNO_3$, respectively.

*Hydrolysis and thermal treatment under inert atmosphere, in the presence of HCl (IN/HCl samples), or without mineral acid (IN/NC samples)*

The procedure was very similar to the one described for the $IN/HNO_3$ samples. The IN/HCl series was obtained from 0.97 g (1.35 mmol) of [FeCl{$Ti_2(OPr^i)_9$}] dissolved in toluene:propan-2-ol (29:58 mL) and added to 29 mL of an aqueous HCl solution (28 mmol $L^{-1}$). The IN/NC samples, in their turn, were produced from a solution of 1.03 g (1.43 mmol) of [FeCl{$Ti_2(OPr^i)_9$}] in toluene:propan-2-ol (31:62 mL), which was added to degassed water (31 mL). Solids obtained after sol-gel processing and drying at 55 °C (yellow for IN55/HCl and brown for IN55/NC), were submitted to thermal treatment in the temperature range of 300-1000 °C.

## Results and Discussion

*$IN/HNO_3$ samples*

Powder XRD data for samples $IN55\text{-}1000/HNO_3$ are presented in Figure 2. Up to 300 °C, only reflections due to anatase $TiO_2$ can be observed.[21] The broad peaks suggest small average crystallite diameters, which were calculated as 4.5 and 5.4 nm for samples $IN55/HNO_3$ and $IN300/HNO_3$, respectively, according to Scherrer's law. Diffraction peaks for hematite (α-$Fe_2O_3$) appear at 500 °C,[22] while the absence of peaks assignable to iron-based phases below this temperature may be due to an amorphous nature of the iron-containing species.

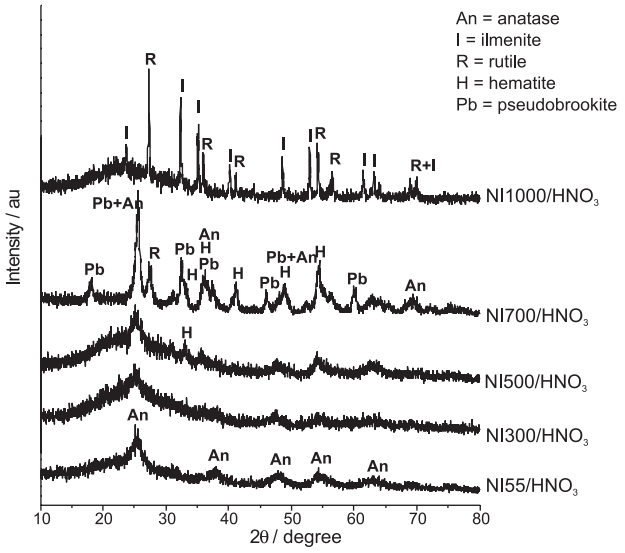


**Figure 2.** Powder X-ray diffractograms for $IN55\text{-}1000/HNO_3$.

A mixture of anatase, rutile, hematite and pseudobrookite was detected at 700 °C.[21,22] These results are similar to those obtained earlier from **1** for reactions carried out in air.[16,17] In the present work, however, the sample $IN700/HNO_3$ still contains anatase at 700 °C, due to an incomplete anatase-rutile phase transition. According to our previous results, only rutile would be detected at 700 °C.[16,17] Therefore, thermal treatment under inert atmosphere apparently contributed to stabilizing the anatase phase, or alternatively to slowing down the phase transition kinetics in $TiO_2$. Additional studies are needed to further clarify this behaviour.

An interesting new finding came from the solid heated to 1000 °C ($IN1000/HNO_3$). The XRD profile revealed the complete absence of peaks assignable to iron(III) species, while new peaks attributed to ilmenite ($FeTiO_3$), a mixed iron(II)-titanium(IV) oxide, were observed.[23]

This implies the reduction of iron(III) in the solid at high temperature, a result not obtained when **1** was submitted to sol-gel processing in air.[16] In addition, all anatase $TiO_2$ was converted to rutile up to this temperature, producing a mixture of rutile and ilmenite (Scheme 1).

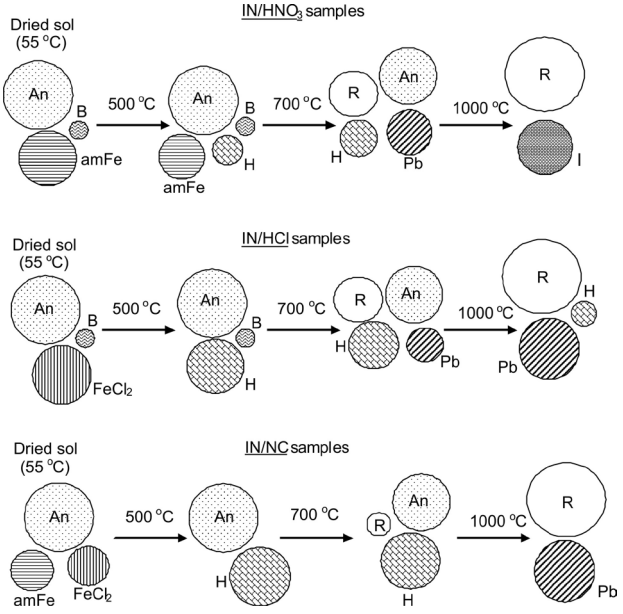


**Scheme 1.** Qualitative representation of the oxide/halide materials identified in the IN/$HNO_3$, IN/HCl and IN/NC samples. An = anatase, B = brookite, R = rutile, $FeCl_2$ = $FeCl_2{\cdot}4H_2O$, amFe = amorphous iron(II)/(III) species, H = hematite, Pb = pseudobrookite and I = ilmenite.

These findings are supported by Raman spectroscopy analysis (Figure 3). Only bands assignable to anatase and brookite are detected up to 300 °C, suggesting that trace amounts of brookite, not observed by XRD (Figure 2), are

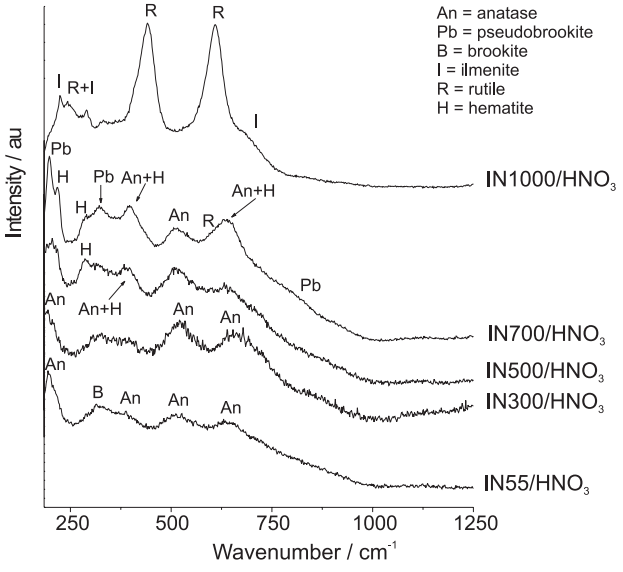


**Figure 3.** Raman spectra for IN55-1000/$HNO_3$.

formed at these temperatures.[21] Bands for hematite appear at 500 °C, while those for a mixture of anatase, rutile, hematite and pseudobrookite are detected at 700 °C.[21,24] Finally, at 1000 °C, the spectrum contains well-defined rutile and low intensity ilmenite bands.[21,24]

The Mössbauer spectra recorded for IN55-700/$HNO_3$ (Figure 4) give Mössbauer parameters in the range for iron(III) oxides (Table 1).[25,26] Results for IN55/$HNO_3$ are compatible with the presence of amorphous $Fe_2O_3$ in the sample. In the solid heat-treated at 300 °C, a doublet with isomer shift (i.s.) and quadrupole splitting (q.s.) values consistent with superparamagnetic hematite particles was detected. The spectrum recorded for IN500/$HNO_3$, in its turn, shows the replacement of the central doublet with a six-line $\alpha$-$Fe_2O_3$ pattern. This is related to the known superparamagnetic $\rightarrow$ ferromagnetic transition typical of hematite: the higher the particle size, the higher the ferromagnetic content and the intensity of the six-line spectrum. In IN700/$HNO_3$, the strong main doublet now presents i.s. and q.s. assignable to pseudobrookite, $Fe_2TiO_5$.[25] Finally, for IN1000/$HNO_3$, a doublet with higher i.s. and q.s. values (Table 1) agrees with the presence of iron(II) in ilmenite, $FeTiO_3$.[26]

**Table 1.** $^{57}$Fe Mössbauer parameters for IN55-1000/$HNO_3$ at 80 K. Isomer shift (i.s.) and quadrupole splitting (q.s.) values are in $mms^{-1}$. Numbers in parentheses correspond to the experimental error in the last significant figure

| Sample / Mössbauer parameter | i.s. | q.s. |
|---|---|---|
| IN55/$HNO_3$ | 0.48(1) | 0.77(2) |
| IN300/$HNO_3$ | 0.40(1) | 0.92(1) |
| IN500/$HNO_3$ | 0.37(2) | 0.92(3) |
| IN700/$HNO_3$ | 0.40(1) | 0.76(1) |
| IN1000/$HNO_3$ | 1.11(1) | 1.01(1) |

EPR spectra recorded for IN55-1000/$HNO_3$ also confirm these findings (Figure 5). Up to 500 °C, the spectra show two main bands with g = 2.0 and 4.3, assigned to iron(III) sites in cubic and distorted rhombic environments, respectively.[27] At 700 °C, weak resonance lines at g = 8.1, 5.6, 4.5, 3.7 and 2.8 are also observed. They are generated by iron(III) substitutionally incorporated into titanium(IV) sites in the rutile lattice, following migration of iron(III) down open channels along the rutile *c*-axis. This leads to the formation of pseudobrookite.[16,17,27] Additionally, a dramatic change was observed at 1000 °C, with the almost complete disappearance of the band at g = 2.0, due to iron(III) in highly symmetric and magnetically concentrated environments, and the emergence of a very broad band between 1500-3000 G. The latter is probably generated by

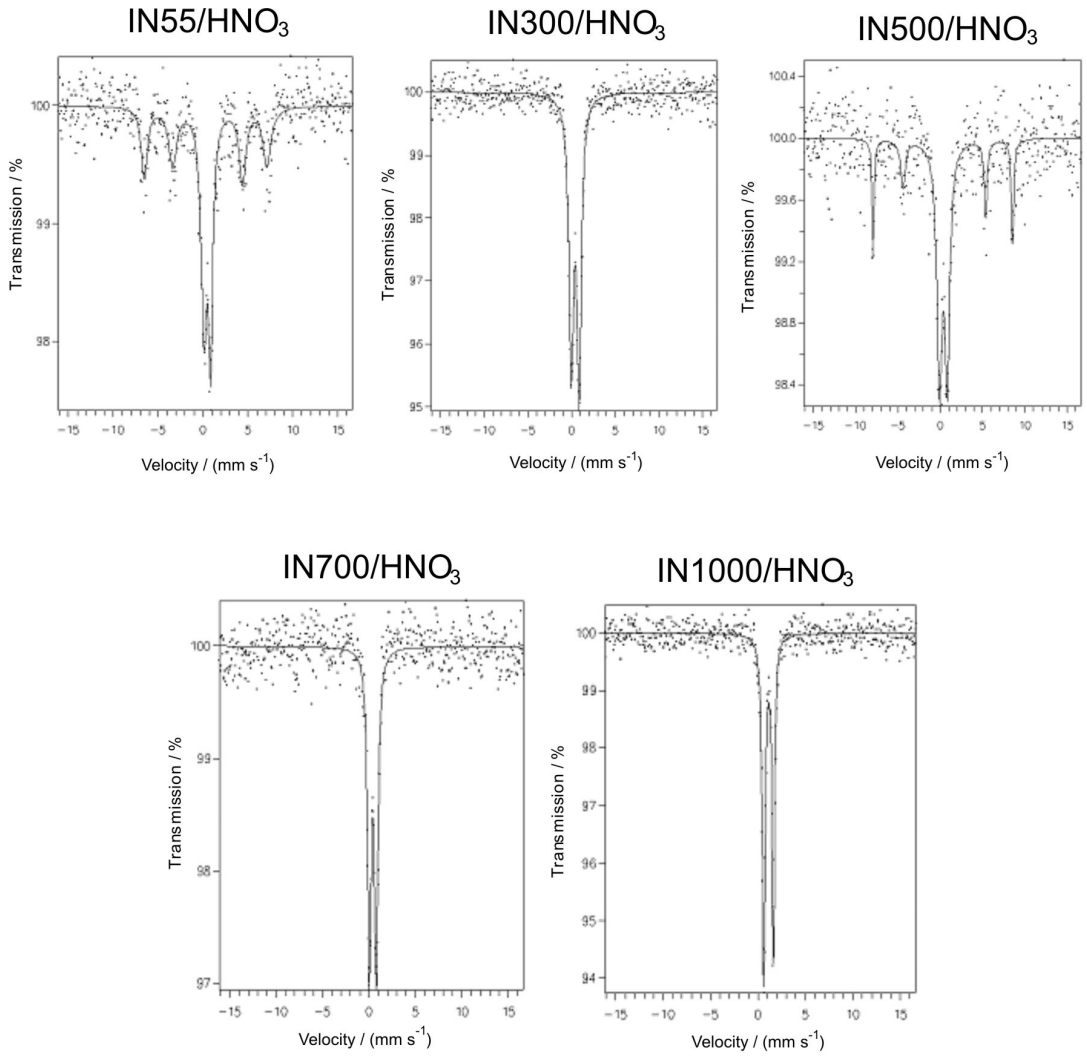


**Figure 4.** Zero field $^{57}$Fe Mössbauer spectra registered at 80 K for IN55-1000/$HNO_3$.

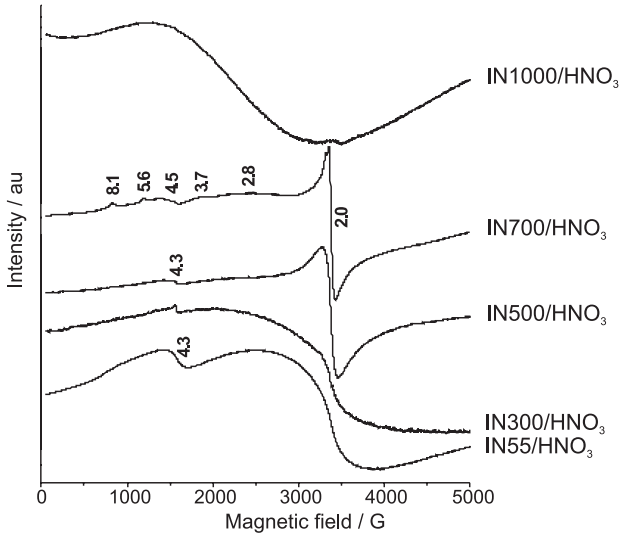


**Figure 5.** EPR spectra registered at 77 K (X-band) for IN55-1000/$HNO_3$. Numbers are for "g" values.

magnetic interaction between iron(II), present in ilmenite, and traces of iron(III) remaining in the solid.

In summary, the use of $HNO_3$, combined with inert atmosphere conditions, in both the sol-gel processing and the thermal treatment of **1**, has led to a mixture of ilmenite and rutile at 1000 °C. Considering the molar proportion of the two metals in the SSP (1Fe:2Ti), which is different from that in either $Fe_2TiO_5$ (pseudobrookite) or $FeTiO_3$ (ilmenite), the formation of both $TiO_2$ and the mixed metal oxide (the latter after thermal treatment) could be explained on stoichiometry grounds.

In spite of the presence of iron(II) in the SSP, the solid products obtained up to 700 °C contained iron(III) oxides, together with titanium(IV) species. Above 700 °C, on the other hand, carbonaceous materials, generated by pyrolysis of organic residues, may have acted as reducing agents in the iron(III)→iron(II) conversion, leading to ilmenite. This finds support in the Raman spectrum recorded for IN700/

$HNO_3$ and IN1000/$HNO_3$ (Figure S1, Supplementary Information), which show very broad bands in the 1200-1700 $cm^{-1}$ range. The pattern of these Raman bands appears to be compatible with the presence of disordered (glassy or amorphous) carbon in the solid.[28] Other workers have arrived at similar results, as for example in the reduction of "$WO_x$" by disordered carbon, during the pyrolysis of tungstic acid in the presence of ammonium polyacrylate at 900 °C.[29]

*IN/HCl samples*

XRD results for IN55-1000/HCl are shown in Figure 6. Sharp diffraction peaks assigned to $FeCl_2 \cdot 4H_2O$ are observed in the sample dried at 55 °C, evidencing that the original oxidation state of the iron centres in **1** was kept in IN55/HCl.[30] Broad peaks attributed to anatase and traces of brookite were also detected at this temperature. Iron oxidation followed heat treatment at 300 °C, as the $FeCl_2 \cdot 4H_2O$ reflections disappeared and new peaks, assigned to hematite, were observed. This may be at least partially rationalized within the grounds of coordination chemistry,[31] because of the high oxidation potential of iron(II) in this very hard, π-donor oxide ($O^{2-}$) environment, known to stabilize metal centres in high oxidation states.[32] π-donor hydroxo ligands have also been reported to favour the oxidation of iron(II) in related systems.[33]

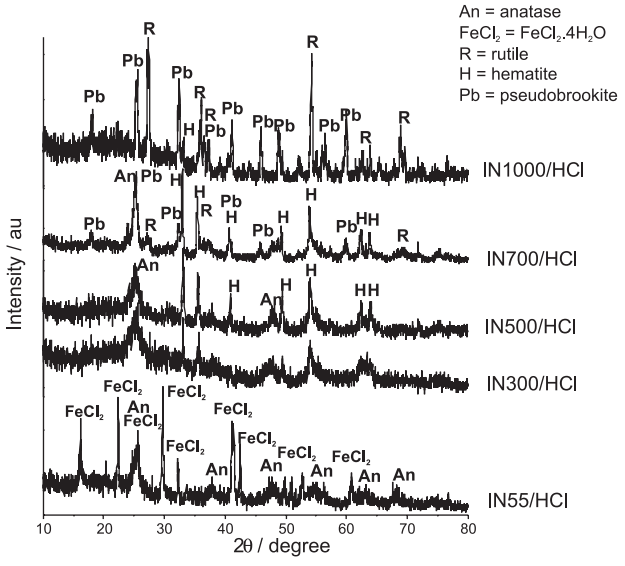


**Figure 6.** Powder X-ray diffractograms for IN55-1000/HCl.

In IN500/HCl, the sharper and more intense hematite peaks indicate higher crystallinity and particle growth. Additional peaks given by pseudobrookite and rutile are detected at 700 °C. Similarly to IN700/$HNO_3$, IN700/HCl shows peaks assignable to anatase, rutile, hematite and pseudobrookite.[21,22] Finally, only pseudobrookite, anatase and hematite are detected in IN1000/HCl. The small relative intensity of the hematite peak located at $2\theta = 33.1°$ indicates a low concentration of α-$Fe_2O_3$ in this sample.

Raman and Mössbauer spectra registered for IN55-1000/HCl (Figures S2-S3 and Table S1 - Supplementary Information) give further support to these considerations.[34] Additionally, Figure S2(b) presents one of the several Raman spectra recorded for the IN700/HCl sample in the range of 180-2000 $cm^{-1}$, showing broad bands assigned to disordered carbon at 1320 and 1580 $cm^{-1}$. We were not able to find a similar, defined two-band pattern in this region for IN1000/HCl; this may suggest combination, oxidation and/or some loss of carbon after thermal treatment at high temperature in the IN/HCl series. The Mössbauer spectrum registered for IN55/HCl contains a doublet whose i.s. and q.s. values are clearly consistent with those expected for $FeCl_2 \cdot 4H_2O$ (Figure S3).[35] A weaker feature is also observed in this spectrum; it probably comes from a small amount of iron(III) in the solid. This illustrates the difficulty in maintaining the oxidation state +II in the chemical system employed in this work.

Therefore, the use of HCl has led to the production of an iron(II) phase at 55 °C, which was not formed when the process was carried out in the presence of $HNO_3$. This is consistent with HCl not being an oxidizing agent for the iron(II) centres provided by **1** in our reaction conditions.

Despite this, the characterisation of IN300/HCl indicates that iron(II) was completely oxidized above 55 °C. This may be related to a recent study by Haderlein and co-workers, also carried out under inert atmosphere.[33] In their report, the reactivity of iron(II) for the reduction of environmentally relevant organic pollutants was compared, under similar experimental conditions, in suspensions of a number of $Fe^{II}/Fe^{III}$-containing minerals, *e.g.*, siderite ($FeCO_3$), hematite, goethite (R-FeOOH), magnetite ($Fe_3O_4$) and pyrite ($FeS_2$). As a general trend, reaction rates for the redox reaction increased in the order $Fe^{II}$ + siderite < $Fe^{II}$ + iron oxides < $Fe^{II}$ + iron sulphides. The low reactivity of $Fe^{II}$ at the siderite surface was explained by stabilization of $Fe^{II}$ compared to $Fe^{III}$ within $FeCO_3$. The high reactivity of FeS or $FeS_2$, on the other hand, was attributed to the redox activity of the sulfide or disulphide ligands.[33] The reactivity of iron(II) at the surface of iron(II)/(III) oxides was intermediate between these extremes.

We may be able to establish a parallel with the systems described in the present work, where iron(II) centres on the surface of titanium(IV) oxides may have acted as electron-donors to organic fragments present in the reaction mixture. These fragments could be reminiscent from solvent

molecules or from organic ligands originally present in the SSP. In the absence of $O_2$, the elimination of carbon as $CO_2$ from the heat-treated sol-gel products is not as favoured as in air, and organic residues probably remain in the products. Temperatures higher than 55 °C may speed up electron-transfer involving the $Fe^{II} \rightarrow Fe^{III}$ half reaction. Also, this redox process would be thermodynamically favoured by formation of hard-hard interactions between the resulting iron(III) and oxide ions.[33] This hypothesis apparently finds support in the SEM/EDS studies discussed below.

*IN/NC samples*

Results of XRD analysis obtained for IN55-1000/NC are similar to those registered for IN55-1000/HCl (Figure S4, Supplementary Information). Once again, a mixture of crystalline anatase and $FeCl_2 \cdot 4H_2O$ was produced in the solid dried under vacuum at 55 °C. The amount of iron(II) chloride tetrahydrate produced in this system was smaller than in IN55/HCl, because in the NC series the trinuclear precursor (**1**) was the only source of both $Fe^{II}$ and $Cl^-$ for the formation of $FeCl_2$, providing them in 1:1 proportion. The chloride content was thus limiting to this conversion, and the remaining iron probably gave rise to amorphous ferrous or ferric oxides/hydroxides (Scheme 1). Raman bands at *ca.* 220-300 $cm^{-1}$ for IN55/NC (Figure S5, Supplementary Information) give support to the presence of $Fe_2O_3$.[24] The comparison of Figures 6 and S4, together with the observation of Figures S2 and S5, indicate that the lack of added HCl favours the oxidation of iron(II), which appears as $Fe^{III}$ in hematite (in the NC series) even at 55 °C. This is probably because, in this condition, the available counter ions to the iron ($OH^-$ or $O^{2-}$) are hard donors that preferably stabilize iron(III) in detriment of iron(II).[31]

In the temperature range of 300-500 °C, diffraction peaks and Raman scattering bands assigned to crystalline hematite and anatase were detected. Hematite, anatase and rutile were observed at 700 °C. Finally, the IN1000/NC solid contains only rutile and pseudobrookite (Scheme 1).[21,22,24]

*SEM/EDS investigations*

SEM images for IN700/$HNO_3$, taken as representative of the lower temperature samples obtained in the presence of $HNO_3$, are presented in Figure 7. Additionally, micrographs obtained for IN1000/$HNO_3$, IN1000/HCl and IN1000/NC are displayed in Figure 8. Images show large and porous agglomerates of smaller particles with no specific regular shape.

The EDS semi-quantitative results obtained for IN55/$HNO_3$ and IN1000/$HNO_3$ (Tables 2 and 3) show that both solids contain variable and relatively high carbon contents, with *ca.* 17% as an average value (note the high standard deviations). As mentioned earlier, these probably derive from solvents and organic hydrolysis products present in the sol-gel media, which were not eliminated as $CO_2$ during the thermal treatment in the oxygen-deficient environment. In IN1000/$HNO_3$, the pyrolysis of the remaining organic groups probably generated low oxidation state carbonaceous species, which caused the observed iron(III) reduction and led to ilmenite. This is supported by EDS data, as the average carbon content in both IN55/$HNO_3$ and IN1000/$HNO_3$ is higher than the average iron content in the same samples (*ca.* 9%, also with high standard deviation). This is compatible with the practically complete reduction of iron(III) in the solid.

EDS results for IN1000/$HNO_3$ show an additional intriguing feature. According to data presented in Table 3, this product shows a marked heterogeneity in elemental distribution, particularly when compared with solids produced from **1** after thermal treatment in air, also at 1000 °C and in the presence of $HNO_3$.[16,17] In that case, EDS analyses performed on different grains gave Ti:Fe:O

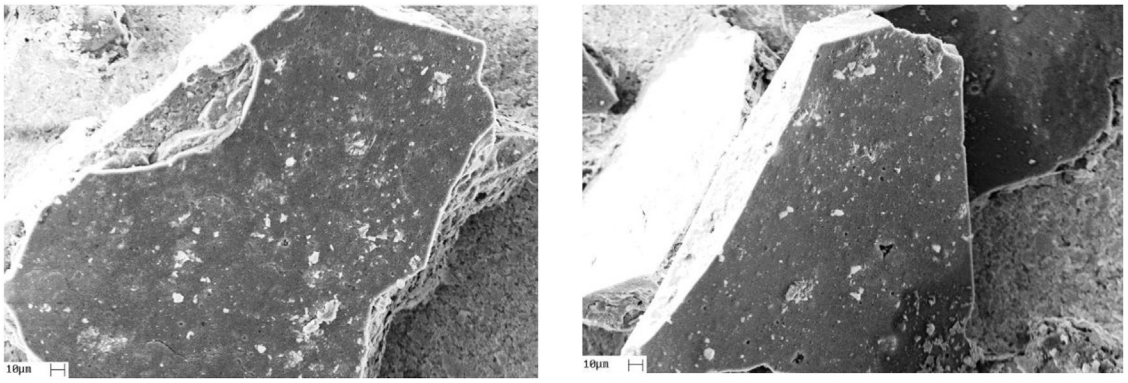


**Figure 7.** SEM micrographs for IN700/$HNO_3$, showing the porous nature of representative grains.

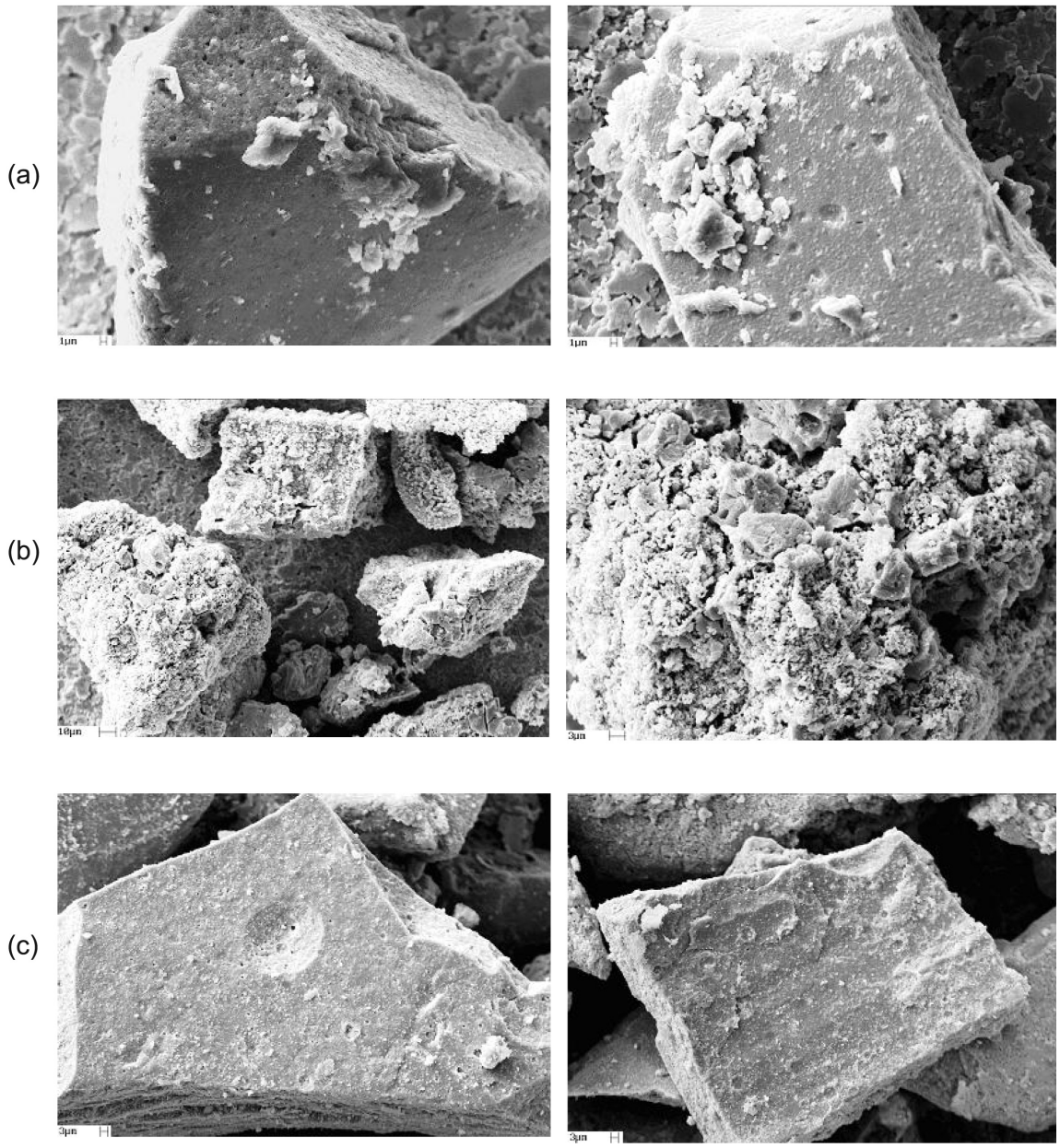


**Figure 8.** SEM micrographs for representative grains of (a) IN1000/$HNO_3$, (b) IN1000/HCl and (c) IN1000/NC.

**Table 2.** EDS experimental composition of IN55/$HNO_3$ [a,b]

| Sample | Atomic Percentage | | | | Atomic ratio | | |
|---|---|---|---|---|---|---|---|
| | O | Ti | Fe | C | O | Ti | Fe |
| Grain 1 | 63.18 | 26.93 | 9.90 | 8.78 | 6.38 | 2.72 | 1 |
| Grain 2 | 73.30 | 19.43 | 7.27 | 12.44 | 10.08 | 2.67 | 1 |
| Grain 3 | 79.71 | 12.39 | 7.90 | 17.48 | 10.09 | 1.57 | 1 |
| Average values | 72.06 | 19.58 | 8.36 | 12.90 | 8.85 | 2.32 | 1 |
| SD [c] | 8.33 | 7.27 | 1.37 | 4.37 | 2.14 | 0.65 | - |

[a]This table does not present an empirical formulation for the IN55/$HNO_3$ solid, as the chemical identity of the iron(III) component is unknown. [b]Added O, Ti and Fe atomic percentages were normalized to 100% (not considering carbon) in order to allow a straightforward comparison of the atomic ratios in different grains. [c]SD = standard deviation.

**Table 3.** EDS experimental composition of IN1000/$HNO_3$ [a]

| Sample | Atomic Percentage | | | | Atomic ratio | | | Empirical composition [b] |
|---|---|---|---|---|---|---|---|---|
| | O | Ti | Fe | C | O | Ti | Fe | |
| Grain 1 | 66.36 | 22.53 | 11.11 | 22.83 | 5.98 | 2.03 | 1 | $FeTiO_3 \cdot 1TiO_2$ |
| Grain 2 | 67.42 | 29.58 | 3.00 | 39.43 | 22.50 | 9.87 | 1 | $FeTiO_3 \cdot 9TiO_2$ |
| Grain 3 | 53.52 | 39.33 | 7.15 | 43.37 | 7.48 | 5.50 | 1 | $FeTiO_3 \cdot 4TiO_2$ |
| Grain 4 | 73.92 | 24.84 | 1.24 | 38.00 | 59.50 | 20.00 | 1 | $FeTiO_3 \cdot 19TiO_2$ |
| Grain 5 | 58.86 | 28.00 | 13.13 | 34.29 | 4.48 | 2.13 | 1 | $FeTiO_3 \cdot 1TiO_2$ |
| Grain 6 | 46.19 | 32.27 | 21.54 | 0.83 | 2.14 | 1.50 | 1 | $2FeTiO_3 \cdot 1TiO_2$ |
| Grain 7 | 48.76 | 30.81 | 20.43 | 15.20 | 2.39 | 1.51 | 1 | $2FeTiO_3 \cdot 1TiO_2$ |
| Grain 8 | 48.28 | 32.56 | 19.16 | 18.70 | 2.52 | 1.70 | 1 | $3FeTiO_3 \cdot 2TiO_2$ |
| Grain 9 | 46.33 | 48.53 | 5.14 | 13.30 | 9.01 | 9.44 | 1 | $FeTiO_3 \cdot 9TiO_2$ |
| Grain 10 | 66.51 | 28.67 | 4.82 | 14.90 | 13.8 | 5.95 | 1 | $FeTiO_3 \cdot 5TiO_2$ |
| Grain 11 | 63.77 | 26.77 | 9.45 | 5.00 | 6.74 | 2.83 | 1 | $FeTiO_3 \cdot 2TiO_2$ |
| Grain 12 | 63.64 | 26.91 | 9.45 | 5.2 | 6.73 | 2.85 | 1 | $FeTiO_3 \cdot 2TiO_2$ |
| Average values | 58.63 | 30.90 | 10.47 | 20.92 | 11.94 | 5.44 | 1 | $FeTiO_3 \cdot 4TiO_2$ |
| SD [c] | 9.63 | 7.02 | 6.87 | 14.64 | 16.03 | 5.47 | - | - |

[a] Added O, Ti and Fe atomic percentages were normalized to 100% (not considering carbon) in order to allow a straightforward comparison of the atomic ratios in different grains. [b] Assuming complete conversion of iron to $FeTiO_3$. [c] SD = standard deviation.

ratios very close to the proportion $3(TiO_2):1(Fe_2TiO_5)$, corresponding to the original 2:1 titanium:iron ratio in the molecular precursor, and confirming the stoichiometric conversion of **1** to the corresponding oxides. In the present work, however, each grain analyzed in IN1000/$HNO_3$ has a different empirical composition, calculated from the Ti, Fe and O weight percentages. For example, there are IN1000/$HNO_3$ grains containing 2, 4, 5, 9 and even 19 equivalents of $TiO_2$ *per* mol of $FeTiO_3$.

In order to further investigate this effect, we carried out similar EDS measurements for samples IN1000/HCl and IN1000/NC; results are presented in Tables 4 and 5. They also reveal heterogeneity in both samples, although much lower than in IN1000/$HNO_3$. In IN1000/HCl, for example, there are grains containing only pseudobrookite ($Fe_2TiO_5$), together with grains with 1, 2 or 3 equivalents of $TiO_2$. In IN1000/NC, in its turn, grains with 2 or 3 equivalents of $TiO_2$ *per* mol of $Fe_2TiO_5$ have been observed. Heterogeneity seems to be the lowest in the solid produced without acid (IN1000/NC), which is also the one better approaching the metal proportion originally present in the SSP (1Fe:2Ti), according to Tables 3-5. This suggests a negative effect of the presence of mineral acids, together with the high carbon contents, over product homogeneity in this particular system, perhaps because they enhance differences in pathways of oxide formation from the Fe and Ti centres in the $O_2$-deficient medium. In this context one could remember that, in spite of being a single-source precursor, **1** contains iron and titanium in different oxidation states and chemical environments (Figure 1). These could be distinct enough to determine, in the severely $O_2$-limited media, different reaction pathways contributing to metal segregation.

Another singular feature is expressed in Tables 4 and 5, concerning the oxygen contents in the absence of nitric acid. These are clearly below the expected values for samples IN1000/HCl and IN1000/NC, calculated from the empirical compositions with the metals as the limiting species. This suggests the production of non-stoichiometric, oxygen-deficient solids from the IN/HCl and IN/NC processing media, and differs from data obtained in the presence of $HNO_3$ (Table 3). Such a result might suggest that nitric acid contributes to oxygen retention in the solids, possibly by a mechanism involving impaired migration of oxygen ions through the bulk. A related report has been made recently by Zhou *et al.*,[36] who observed a significant detrimental effect of $HNO_3$ on oxygen permeation through a dense mixed metal oxide membrane employed as the cathode in solid oxide fuel cells. In this type of system, an oxygen molecule first adsorbs over the membrane surface on the oxygen-rich side, where it dissociates into oxygen ions and generates electron holes, both of which then migrate through the bulk to the other side of the membrane surface. There they recombine into an oxygen molecule, which finally desorbs and evolves into the oxygen-poor side. According to these authors, the use of nitric acid in the mixed metal oxide synthesis led to the decrease of crystallite size, increase of sintering during fabrication, and reduced

**Table 4.** EDS experimental composition of IN1000/HCl [a]

| Sample | Atomic Percentage | | | | Atomic ratio | | | Empirical composition [b] |
|---|---|---|---|---|---|---|---|---|
| | O | Ti | Fe | C | O | Ti | Fe | |
| Grain 1 | 57.68 | 20.75 | 21.57 | 1.74 | 2.78 | 1 | 1.04 | $Fe_2TiO_5 \cdot 1TiO_2$ |
| Grain 2 | 55.53 | 20.55 | 23.93 | 4.13 | 2.70 | 1 | 1.16 | $Fe_2TiO_5 \cdot 1TiO_2$ |
| Grain 3 | 49.80 | 24.65 | 25.55 | 0.17 | 2.02 | 1 | 1.04 | $Fe_2TiO_5 \cdot 1TiO_2$ |
| Grain 4 | 60.07 | 27.75 | 12.18 | 6.33 | 4.93 | 2.28 | 1 | $Fe_2TiO_5 \cdot 3TiO_2$ |
| Grain 5 | 58.77 | 17.87 | 23.35 | 4.82 | 3.29 | 1 | 1.31 | $Fe_2TiO_5 \cdot 1TiO_2$ |
| Grain 6 | 48.50 | 14.30 | 37.20 | 6.47 | 3.39 | 1 | 2.60 | $3Fe_2TiO_5 \cdot 1Fe_2O_3$ |
| Grain 7 | 46.43 | 18.90 | 34.67 | 3.06 | 2.46 | 1 | 1.83 | $Fe_2TiO_5$ |
| Grain 8 | 55.92 | 22.91 | 21.17 | 4.86 | 2.64 | 1.08 | 1 | $Fe_2TiO_5 \cdot 1TiO_2$ |
| Grain 9 | 49.42 | 21.50 | 29.08 | 7.34 | 2.30 | 1 | 1.35 | $Fe_2TiO_5 \cdot 1TiO_2$ |
| Grain 10 | 48.51 | 13.98 | 37.51 | 2.33 | 3.47 | 1 | 2.68 | $3Fe_2TiO_5 \cdot 1Fe_2O_3$ |
| Grain 11 | 58.22 | 24.38 | 17.40 | 5.22 | 3.35 | 1.40 | 1 | $Fe_2TiO_5 \cdot 2TiO_2$ |
| Average values | 53.53 | 20.69 | 25.78 | 4.22 | 3.03 | 1.16 | 1.46 | $Fe_2TiO_5 \cdot 1TiO_2$ |
| SD [(c)] | 5.01 | 4.26 | 8.13 | 2.20 | 0.79 | 0.39 | 0.64 | - |

[a]Added O, Ti and Fe atomic percentages were normalized to 100% (not considering carbon) in order to allow a straightforward comparison of the atomic ratios in different grains. [b]Assuming complete conversion of iron to $Fe_2TiO_5$. [c]SD = standard deviation.

**Table 5.** EDS experimental composition of IN1000/NC [a]

| Sample | Atomic Percentage | | | | Atomic Ratio | | | Empirical composition [b] |
|---|---|---|---|---|---|---|---|---|
| | O | Ti | Fe | C | O | Ti | Fe | |
| Grain 1 | 47.70 | 32.58 | 19.72 | 0.13 | 2.42 | 1.65 | 1 | $Fe_2TiO_5 \cdot 2TiO_2$ |
| Grain 2 | 50.41 | 31.19 | 18.41 | 2.76 | 2.74 | 1.69 | 1 | $Fe_2TiO_5 \cdot 2TiO_2$ |
| Grain 3 | 73.37 | 15.27 | 11.36 | 8.32 | 6.46 | 1.34 | 1 | $Fe_2TiO_5 \cdot 2TiO_2$ |
| Grain 4 | 53.41 | 28.61 | 17.97 | 8.12 | 2.97 | 1.59 | 1 | $Fe_2TiO_5 \cdot 2TiO_2$ |
| Grain 5 | 63.66 | 23.92 | 12.42 | 1.73 | 5.12 | 1.93 | 1 | $Fe_2TiO_5 \cdot 3TiO_2$ |
| Grain 6 | 68.22 | 18.15 | 13.63 | 12.17 | 5.01 | 1.33 | 1 | $Fe_2TiO_5 \cdot 2TiO_2$ |
| Grain 7 | 72.16 | 17.41 | 10.43 | 17.86 | 6.92 | 1.67 | 1 | $Fe_2TiO_5 \cdot 2TiO_2$ |
| Grain 8 | 44.39 | 33.90 | 21.72 | 0.20 | 2.04 | 1.56 | 1 | $Fe_2TiO_5 \cdot 2TiO_2$ |
| Grain 9 | 54.60 | 29.28 | 16.12 | 0.62 | 3.39 | 1.82 | 1 | $Fe_2TiO_5 \cdot 3TiO_2$ |
| Grain 10 | 46.91 | 32.85 | 20.25 | 6.48 | 2.32 | 1.62 | 1 | $Fe_2TiO_5 \cdot 2TiO_2$ |
| Grain 11 | 63.47 | 20.91 | 15.62 | 10.21 | 4.06 | 1.34 | 1 | $Fe_2TiO_5 \cdot 2TiO_2$ |
| Grain 12 | 42.04 | 36.05 | 21.91 | 13.90 | 1.92 | 1.65 | 1 | $Fe_2TiO_5 \cdot 2TiO_2$ |
| Grain 13 | 43.42 | 35.50 | 21.08 | 6.99 | 2.06 | 1.68 | 1 | $Fe_2TiO_5 \cdot 2TiO_2$ |
| Average values | 55.67 | 27.36 | 16.97 | 6.88 | 3.65 | 1.61 | 1 | $Fe_2TiO_5 \cdot 2TiO_2$ |
| SD [c] | 11.20 | 7.33 | 4.02 | 5.67 | 1.72 | 0.18 | - | - |

[a]Two distinct measurements were performed for each grain. Also, in these samples, added O, Ti and Fe atomic percentages were normalized to 100% (not considering carbon) in order to allow a straightforward comparison of the atomic ratios in different grains. [b]Assuming complete conversion of iron to $Fe_2TiO_5$. [c]SD = standard deviation.

surface oxygen exchange kinetics and bulk diffusion rate in the cell cathode.[36] This behaviour has been correlated with the higher sinterability of ceramics produced in the presence of $HNO_3$,[36,37] which show lower grain porosity after heat treatment and a decreased effective surface area for reactions carried out after sintering.

Ardizzone *et al.*[38] have also shown that different counter ions to $Fe^{III}$ ($NO_3^-$, $Cl^-$ and $SO_4^{2-}$) in the sol-gel preparation of iron-doped zircon pigments led to crystallite sizes and BET surface area dependant on the anionic partner, being both significantly smaller for $NO_3^-$ than for $Cl^-$ or $SO_4^{2-}$. The thermal stability of the anions and the nature of the

chemical interaction between them and the metal centres have been evoked to account for these findings, though not in a conclusive way.[37,38] Additionally, Collón *et al.*[37] reported that the pre-treatment of $TiO_2$ with nitric acid, as compared with $H_2SO_4$ or $H_3PO_4$ (and even to untreated $TiO_2$), failed to stabilise the photocatalyst against sintering as calcination temperature increased, leading to a drastic decay in the BET surface area and to the early, undesired rutilization of the catalyst.

In the present work, there appears to be a correlation between oxygen and carbon retention in the solids prepared with $HNO_3$, as they present both higher oxygen content and average carbon percentage roughly 3-5 times larger than the related IN/HCl and the IN/NC samples (Tables 3-5). We have not yet found a satisfactory explanation for this finding, nor have we encountered any mention to a similar behaviour in the literature. We believe that the full understanding of this result depends on the elucidation of the chemical nature of these oxygen- and carbon-containing species, their interactions with the oxide matrix, and their mobility through the bulk and to the surface of the grains. Additional data on similar sol-gel systems processed under inert atmosphere are also needed for comparison. Both lines of work continue under investigation in our laboratory.

Finally, dioxygen loss at elevated temperatures in low $pO_2$ atmospheres is expected to generate point defects (oxygen vacancies) in oxide lattices:[39,40]

$$O_{O^{2-}}^{2-} \longrightarrow 1/2\ O_{2(g)} + (V_{O^{2-}})^{\bullet\bullet} + 2\ e'$$

As a number of properties associated with oxides - such as electrical conductivity and diffusivity of ions - are associated with lattice defects and their concentration in the bulk solid, this occurrence can alter or enhance product features.

In the present work, the observed oxygen deficiency may have contributed to the heterogeneity observed in the solids heat-treated under inert atmosphere. This is because oxygen vacancies in the oxide lattice may have affected the mobility of the iron and titanium cations. According to Dieckmann,[40] a number of different factors, such as defect concentration, size of the moving ions and electrostatic interactions between the ions and their surroundings, may affect the diffusivity of an ion on a crystal lattice. Also, both the size of the ion and the strength of its electrostatic interactions with the lattice depend on its charge state. In this context, $Ti^{IV}$ presents higher positive charge density and smaller ionic radius than high spin $Fe^{II}$ or $Fe^{III}$. Therefore, it may be reasonable to expect different titanium and iron mobilities in areas with different concentration of defects, contributing to partial metal segregation throughout the material.[40]

## Conclusions

Significant differences were observed when the sol-gel and thermal treatments of $[FeCl\{Ti_2(OPr^i)_9\}]$ (**1**) were performed in air[16,17,19] and under inert atmosphere. In the present work, the composition of the reaction mixture and the atmosphere of processing had a strong influence on the chemical nature of the final materials, either chloride or oxides, prepared from the SSP. High contents of carbon were detected in all solids and this probably contributed to the production of heterogeneous materials showing a non-uniform elemental distribution. Furthermore, oxygen-deficient products were apparently generated when either HCl or no acid was employed in the processing of the SSP. In these solids, a high concentration of lattice defects (oxygen vacancies) has probably been induced, possibly leading to discrepancies in the ionic mobility of iron(II)/(III) and titanium(IV) ions at high temperatures. Chemical reactivity and physical properties of the materials resulting from these treatments are now under investigation by our group.

## Acknowledgments

We are grateful to MSc Dayane M. Reis, MSc Rúbia C. R. Bottini and Dr. Geraldo R. Friedermann (UFPR) for helpful discussions and for the EPR spectra. This work has been sponsored by the Conselho Nacional de Desenvolvimento Científico e Tecnológico (CNPq), Coordenação de Aperfeiçoamento de Pessoal de Nível Superior (CAPES), Fundação Araucária, Fundação de Amparo à Pesquisa do Estado de São Paulo (FAPESP), Financiadora de Estudos e Projetos (FINEP/MCT/CT-INFRA) and Universidade Federal do Paraná (UFPR). D.J.E. thanks the Biotechnology and Biological Sciences Research Council (UK) for financial support.

## Supplementary Information

Supplementary data (Figures S1-S5 and Table S1) are available free of charge at http://jbcs.sbq.org.br, as a PDF file.

## References

1. Wachs, I. E.; *Catal. Today* **2005**, *100*, 79.
2. Liang, Y. G.; Han, X. Y.; Cong, C.; Yi, Z. H.; Zhou, L. Q.; Sun, J. T.; Zhang, K. L.; Zhou, Y. H.; *Nanotechnology* **2007**, *18*, 135607.
3. Frenzer, G.; Maier, W. F.; *Annu. Rev. Mater. Res.* **2006**, *36*, 281.
4. Lee, J.-H.; Huh, Y.-M.; Jun, Y.-W.; Seo, J.-W.; Jang, J.; Song, H.-T.; Kim, S.; Cho, E.-J.; Yoon, H.-G.; Suh, J.-S.; Cheon, J.; *Nat. Med. (N. Y., NY, U. S.)* **2007**, *13*, 95.

5. Hubert-Pfalzgraf, L. G.; *J. Mater. Chem.* **2004**, *14*, 3113.
6. Kessler, V. G.; *J. Sol-Gel Sci. Technol.* **2004**, *32*, 11.
7. Kessler, V. G.; Spijksma, G. I.; Seisenbaeva, G. A.; Håkansson, S.; Blank, D. H. A.; Bouwmeester, H. J. M.; *J. Sol-Gel Sci. Technol.* **2006**, *40*, 163.
8. Boettcher, S. W.; Fan, J.; Tsung, C.-K.; Shi, Q.; Stucky, G. D.; *Acc. Chem. Res.* **2007**, *40,* 784.
9. Cushing, B. L.; Kolesnichenko, V. L.; O'Connor, C. J.; *Chem. Rev.* **2004**, *104*, 3893.
10. Ismail, A. A.; *Appl. Catal., B* **2005**, *58*, 115.
11. Neri, G.; Rizzo, G.; Galvagno, S.; Loiacono, G.; Donato, A.; Musolino, M. G.; Pietropaolo, R.; Rombi, E.; *Appl. Catal., A* **2004**, *274*, 243.
12. Brethon, A.*;* Hubert-Pfalzgraf, L. G.; Daran, J.-C.; *Dalton Trans.* **2006**, 250; Stéphane, D.; Hubert-Pfalzgraf, L. G.; *Mater. Lett.* **2004**, *58*, 1989.
13. Veith, M.; *J. Chem. Soc., Dalton Trans.* **2002**, 2405; Veith, M.; Haas, M.; Huch, V.; *Chem. Mater.* **2005**, *17*, 95.
14. Mehring, M.; *Coord. Chem. Rev.* **2007**, *251*, 974.
15. Spijksma, G. I.; Kloo, L.; Bouwmeester, H. J. M.; Blank, D. H. A.; Kessler, V. G.; *Inorg. Chim. Acta* **2007**, *360*, 2045.
16. Camargo, P. H. C.; Nunes, G. G.; Friedermann, G. R.; Evans, D. J.; Leigh, G. J.; Tremiliosi-Filho, G.; Sá, E. L. de; Zarbin, A. J. G.; Soares, J. F.; *Mater. Res. Bull.* **2003**, *38*, 1915.
17. Camargo, P. H. C.; Nunes, G. G.; Evans, D. J.; Leigh, G. J.; Tremiliosi-Filho, G.; Sá, E. L.; Zarbin, A. J. G.; Soares, J. F.; *Prog. Colloid Polym. Sci.* **2004**, *128*, 221.
18. Nunes, G. G.; Reis, D. M.; Amorim, P. T.; Sá, E. L.; Mangrich, A. S.; Evans, D. J.; Hitchcock, P. B.; Leigh, G. J.; Nunes, F. S.; Soares, J. F.; *New. J. Chem.* **2002**, *26*, 519.
19. Menezes, W. G.; Camargo, P. H. C.; Oliveira, M. M.; Evans, D. J.; Soares, J. F.; Zarbin, A. J. G.; *J. Colloid Interface Sci.* **2006**, *229*, 291.
20. Perrin, D. D.; Armarego, W. L. F.; *Purification of Laboratory Chemicals*, 3rd ed., Butterworth-Heinemann: Oxford, 1988.
21. Alemany, L. J.; Banares, M. A.; Pardo, E.; Martin-Jiménes, F.; Blasco, J. M.; *Mater. Charact.* **2000**, *44*, 271.
22. Wang, S.; Wang, W.; Wang, W.; Jiao, Z.; Liu, J.; Qian, Y.; *Sens. Actuators, B* **2000**, *69*, 22; Pal, B.; Sharon, M.; Nogami, G.; *Mater. Chem. Phys.* **1999**, *59*, 254.
23. Mona, J.; Kale, S. N.; Gaikwad, A. B.; Murugan, A. V.; Ravi, V.; *Mater. Lett.* **2006**, *60*, 1425.
24. Bersani, D.; Lottici, P.P.; Montenero, A.; *J. Mater. Sci.* **2000**, *35*, 4301; de Faria, D. L. A.; Silva, S. V.; de Oliveira, M. T.; *J. Raman Spectrosc.* **1997**, *28*, 873.
25. Zboril, R.; Mashlan, M.; Petridis, D.; *Chem. Mater.* **2002**, *14*, 969; Bødker, F.; Hansen, M. F.; Koch, C. B.; Lefmann, K.; Mørup, S.; *Phys. Rev. B: Condens. Matter Mater. Phys.* **2000**, *61*, 6826; Howard, D. G.; Nussbaum, R. H.; *Surface Sci.* **1980**, *93*, L105; Benz, M.; Van der Kraan, A.M.; Prins, R.; *Appl. Catal., A* **1998**, *172*, 149.
26. McCammon, C.; *Phase Transitions* **1996**, *58B*, 1.
27. Prakash, C.; Husain, S.; Singh, R. J.; Mollah, S.; *J. Alloys Compd.* **2001**, *326*, 47; Ennas, G.; Musinu, A.; Piccaluga, G.; Zedda, D.; Gatteschi, D.; Sangregorio, C.; Stanger, J. L.; Concas, G.; Spano, G.; *Chem. Mater.* **1998**, *10*, 495; Amorelli, A.; Evans, J. C.; Rowlands, C. C.; Egerton, T. A.; *J. Chem. Soc., Faraday Trans. I* **1987**, *83*, 3541; Schwertmann, U.; Friedi, J.; Pfab, G.; Gehring, A. U.; *Clays Clay Miner.* **1995**, *43*, 599.
28. Chu, P. K.; Li, L.; *Mater. Chem. Phys.* **2006**, *96*, 253.
29. Hudson, M. J.; Peckett, J. W.; Harris, P. J. F.; *J. Mater. Chem.* **2003**, *13*, 445.
30. Lazar, K.; Pal-Borbely, G.; Beyer, H. K.; Karge, H. G.; *J. Chem. Soc., Faraday Trans.* **1994**, *90*, 1329.
31. Ayers, P. W.; Parr, R. G.; Pearson, R. G.; *J. Chem. Phys.* **2006**, *124*, 194107; Ayers, P. W.; *Faraday Discuss.* **2007**, *135*, 161.
32. Carina, R. F.; Verzegnassi, L.; Bernardinelli, G.; Williams, A. F.; *Chem. Commun.* **1998**, 2681.
33. Elsner, M.; Schwarzenbach, R. P.; Haderlein, S. B.; *Environ. Sci. Technol.* **2004**, *38*, 799.
34. Bruni, S.; Cariati, F.; Fermo, P.; Spinolo, G.; Martini, M.; *J. Phys. Chem. Solids* **1998**, *59*, 845.
35. Weidenthaler, C.; Zibrowius, B.; Schimanke, J.; Mao, Y.; Mienert, B.; Bill, E.; Schmidt, W.; *Microporous Mesoporous Mater.* **2005**, *84*, 302; Greenwood, N. N.; Gibb, T. C.; *Mössbauer Spectroscopy*, Chapmann and Hall: London, 1971.
36. Zhou, W.; Ran, R.; Shao, Z. P.; Gu, H. X.; Jin, W. Q.; Xu, N. P.; *J. Power Sources* **2007**, *174*, 237.
37. Colón, G.; Sánchez-España, J. M.; Hidalgo, M. C.; Navío, J. A.; *J. Photochem. Photobiol., A* **2006**, *179*, 20.
38. Ardizzone, S.; Binaghi, L.; Cappelletti, G.; Fermo, P.; Gilardoni, S.; *Phys. Chem. Chem. Phys.* **2002**, *4*, 5683.
39. Halder, N.; Chattopadhyay, D.; das Sharma, A.; Saha, D.; Sen, A.; Maiti, H. S.; *Mater. Res. Bull.* **2001**, *36*, 905.
40. Dieckmann, R.; *J. Phys. Chem. Solids* **1998**, *59*, 507.


*Received: February 13, 2008*
*Web Release Date: September 19, 2008*

**FAPESP helped in meeting the publication costs of this article.**

*J. Braz. Chem. Soc.*, Vol. 19, No. 8, S1-S3, 2008.
Printed in Brazil - ©2008 Sociedade Brasileira de Química
0103 - 5053 $6.00+0.00



# Synthesis of Fe/Ti Oxides from a Single Source Alkoxide Precursor under Inert Atmosphere

***Pedro H. C. Camargo,[a] Giovana G. Nunes,[a] Eduardo L. de Sá,[a] Germano Tremiliosi-Filho,[b] David J. Evans,[c] Aldo J. G. Zarbin[a] and Jaísa F. Soares*[,a]***

*[a]Departamento de Química, Universidade Federal do Paraná, Centro Politécnico, Jardim das Américas, 81530-900 Curitiba-PR, Brazil*

*[b]Instituto de Química de São Carlos, Universidade de São Paulo, 13560-970 São Carlos-SP, Brazil*

*[c]John Innes Centre, Norwich Research Park, Colney, Norwich NR4 7UH, England*

**Table S1.** $^{57}$Fe Mössbauer parameters obtained for IN55-1000/HCl at 80 K. Isomer shift (i.s.) and quadrupole splitting (q.s.) values are in mms$^{-1}$

| Sample/ Mössbauer parameters[a] | i.s. | q.s. |
|---|---|---|
| IN55/HCl | 1.29 | 2.97 |
| IN300/HCl | 0.42 | 0.81 |
| IN700/HCl | 0.45 | 0.72 |
| IN1000/HCl | 0.44 | 0.70 |

[a]No fitting could be achieved for IN500/HCl due to the small mass of the sample and, consequently, the too low spectrum intensity.

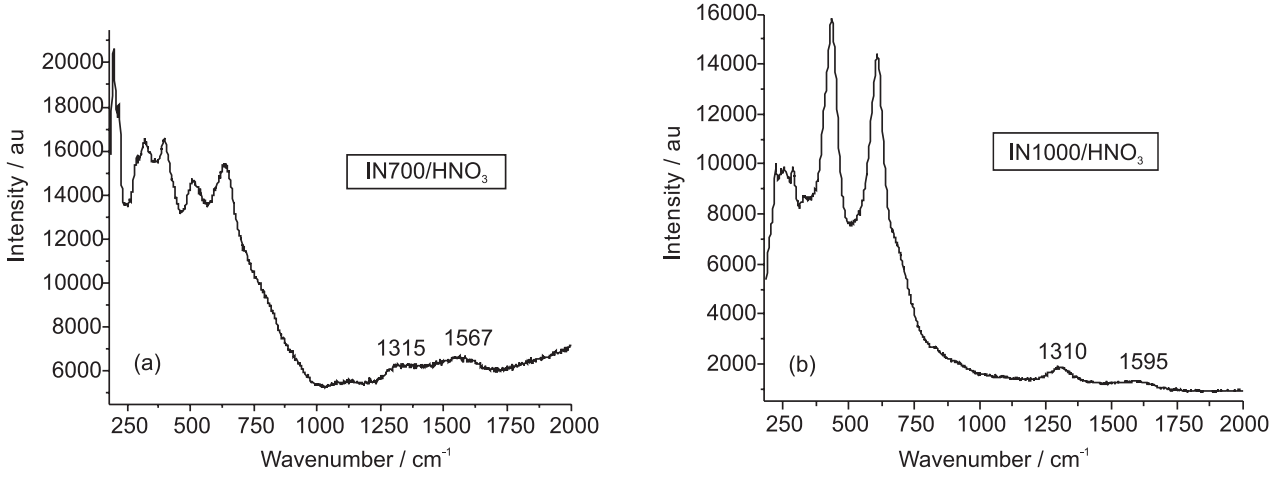


**Figure S1.** Raman spectra for (a) IN700/$HNO_3$ and (b) IN1000/$HNO_3$ in the range of 180-2000 cm$^{-1}$. Bands at 1200-1700 cm$^{-1}$ are possibly related to the presence of disordered carbon in the samples.

*e-mail: jaisa@quimica.ufpr.br

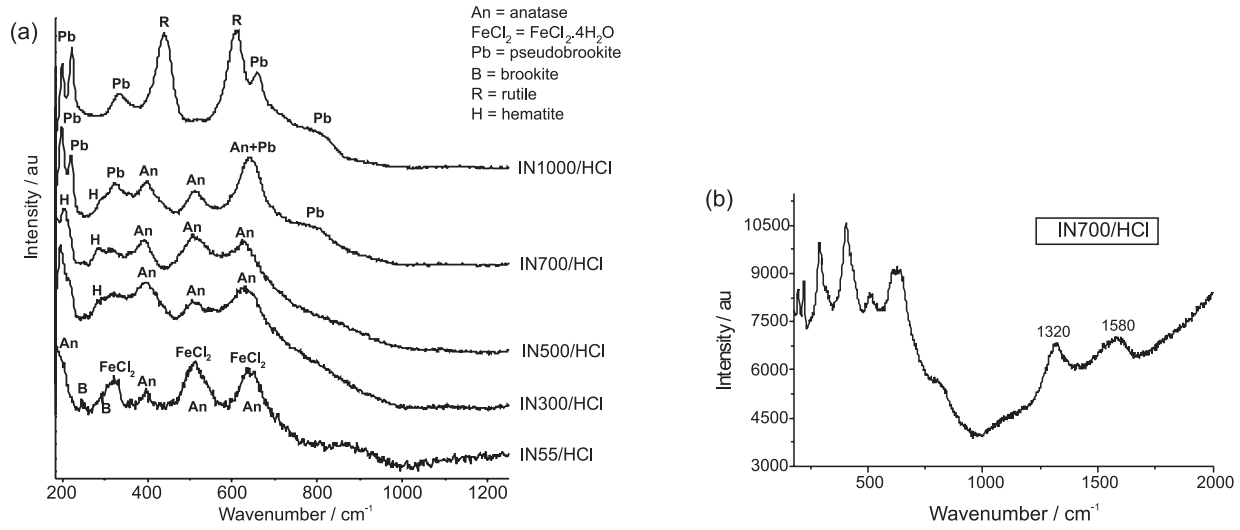


**Figure S2.** (a) Raman spectra for IN55-1000/HCl. (b) Raman spectrum for IN700/HCl in the range of 180-2000 $cm^{-1}$. The broad bands at 1320 and 1580 $cm^{-1}$ are compatible with the presence of disordered carbon.

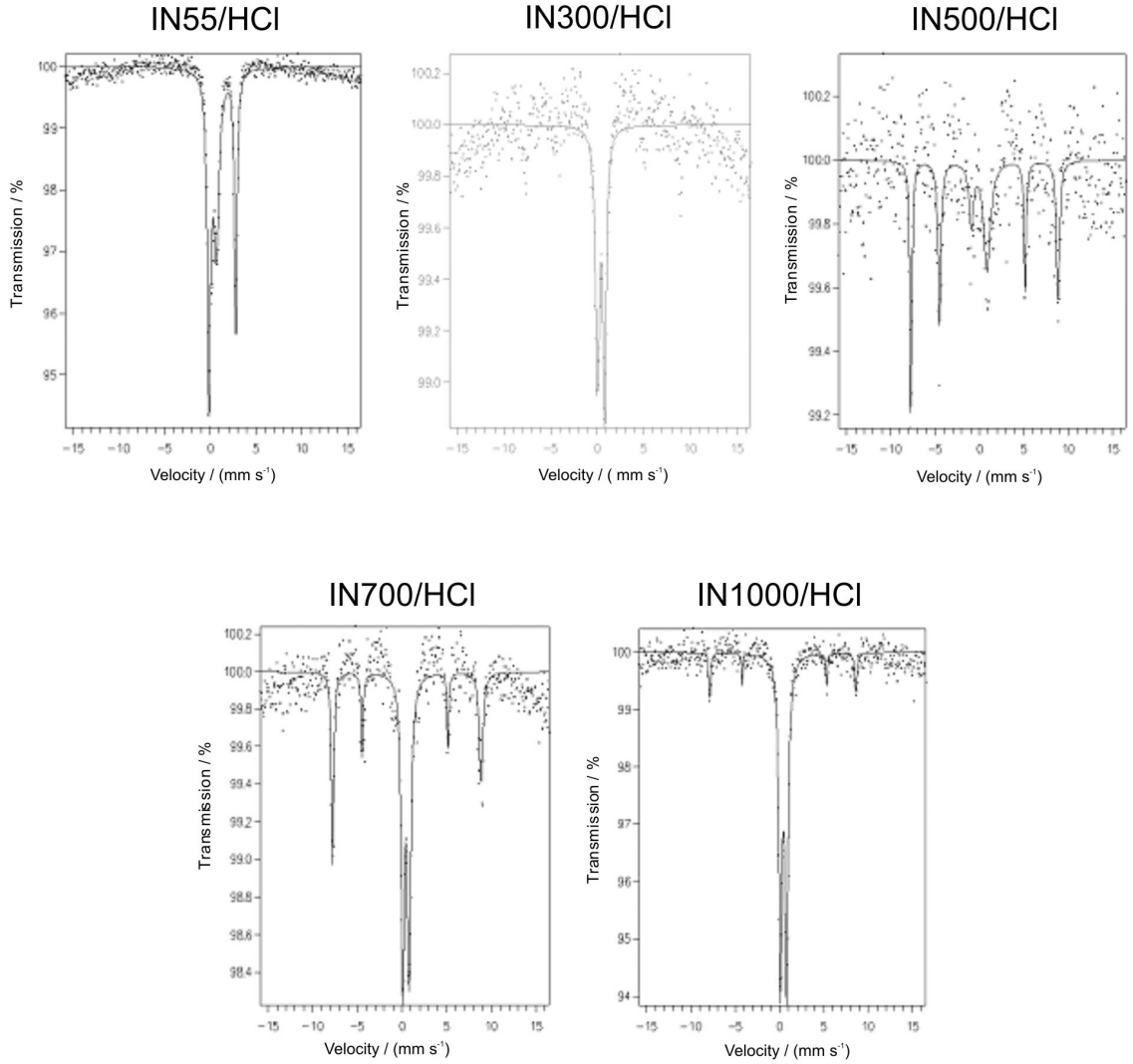


**Figure S3.** Zero field $^{57}Fe$ Mössbauer spectra registered at 80 K for IN55-1000/HCl. Some spectra have low signal/noise ratios, because of the small amount of sample available for analysis.

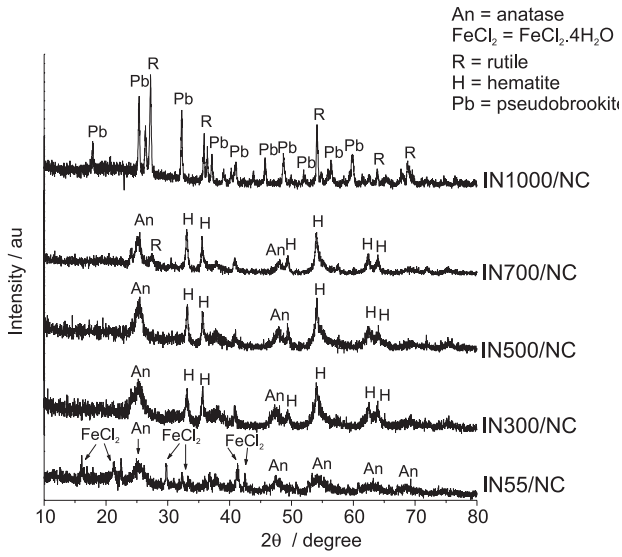


**Figure S4.** Powder X-ray diffractograms for IN55-1000/NC.

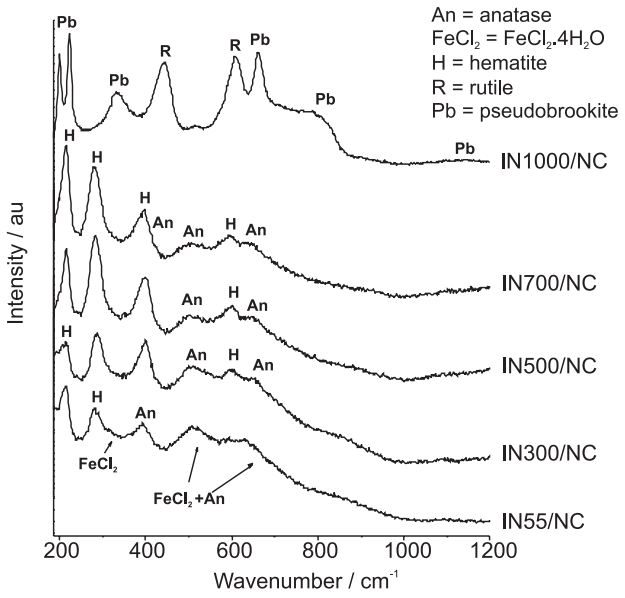


**Figure S5.** Raman spectra for IN55-1000/NC.